Universidad de La Laguna

Facultad de Ciencias, Sección de Física

Máster Universitario en Astrofísica

TRABAJO DE FIN DE MÁSTER

Development of a numerical model for star formation at low resolution

Alex Massaro Achá

Tutor:

Dr. Claudio Dalla Vecchia

Co-tutor:

M.Sc. Isaac Alonso Asensio

Marzo, 2020

Contents

Abstract

The present Master's thesis is concerned with the development and assessment of a prescription to model star formation in the low numerical resolution regime of cosmological hydrodynamical simulations.

A study is made of previously introduced prescriptions in order to understand their physical motivations and to identify the features that cause them to produce different outcomes when changes to numerical resolution are made. It is found that these prescriptions are based on a combination of theoretical and observational findings related to the multiphase nature of the interstellar medium, and the conditions under which a cloud becomes gravitationally unstable upon a phase transition from atomic to molecular composition. Additionally, empirical correlations in the form of star formation laws obligate these prescriptions to rely on local hydrodynamical properties of the cosmic gas in order to form stars in the simulations. This reliance unavoidably renders them resolution-dependent. In general, whenever a prescription to model unresolved physical processes in a cosmological hydrodynamical simulation makes use of local hydrodynamical properties, it is expected that its outcomes will be different for different numerical resolutions.

On the basis of this difficulty, a new prescription has to be sought whenever a cosmological hydrodynamical simulation is intended to be run with an unprecedented numerical resolution, regardless of whether it is to the high or low end. For instance, simulations that aim to sample a larger volume of the Universe, in comparison with what its typically done, must adjust their numerical resolution to the low end in order to keep computational demands manageable. Hence, they require a prescription for star formation that is well-behaved in this regime.

Different procedures to arrive at such a prescription were taken into account, which led to different alternatives being devised. Considering that this is a subject that has been scarcely studied previously in the literature, attention is focused on the alternative that can provide the simplest recipe. Accordingly, a procedure is used that enables a connection to be established between simulations of different numerical resolutions, through which a number of insights can be gained about unresolved properties in low resolution simulations; in a statistical sense, evidently. This properties can then be used to form stars in said simulations.

Having selected the simplest alternative, it was implemented in the public version of the Arepo code for cosmological hydrodynamical simulations, and a series of simulations were run in order to assess the degree to which this alternative is able to overcome the difficulties of previously developed prescriptions. The results found certainly look promising; however, more in-depth studies are required to complement the assessment in regimes where the current work is inadequate.

Resumen

El presente Trabajo de Fin de Máster se concierne con el desarrollo y evaluación de una prescripción para modelar la formación de estrellas en simulaciones cosmológicas de baja resolución numérica.

Se realiza un estudio de prescripciones introducidas con anterioridad con el objetivo de entender sus fundamentos físicos e identificar las características que hacen que sus resultados sean diferentes dependiendo de la resolución numérica empleada. Se encuentra que dichas prescripciones se basan en hallazgos tanto teóricos como observacionales relacionados con las múltiples fases que coexisten en el medio interestelar, y con las condiciones bajo las cuales una nube se vuelve inestable gravitacionalmente cuando ocurre una transición de fase por la cual gas atómico se convierte en gas molecular. Adicionalmente, correlaciones empíricas bajo la forma de leyes de formación estelar obligan a estas prescripciones a depender de propiedades hidrodinámicas locales del gas cósmico para poder formar estrellas en la simulación. Esta dependencia se traduce inevitablemente en una dependencia con la resolución numérica. En general, siempre que una prescripción que modela un proceso físico no resuelto en una simuación cosmológica dependa de propiedades hidrodinámicas locales, es de esperar que los resultados de dicha prescripción dependan también de la resolución numérica empleada.

Debido a esta dificultad, cada vez que se pretenda correr una simulación cosmológica que tenga una resolución numérica nunca antes empleada, ya sea alta o baja, se deberá buscar una nueva prescripción para poder formar estrellas en ella. Por ejemplo, simulaciones que deseen modelar una mayor región del Universo, en comparación con las que típicamente se consideran, deben recurrir a menores resoluciones numéricas de tal forma que la carga computacional se mantenga manejable. Como consecuencia, dichas simulaciones requieren de una prescripción de formación de estrellas que sea bien comportada en este régimen.

Se consideraron diferentes procedimientos para obtener dicha prescripción, lo cual conllevo a que se identificasen diferentes alternativas. Dado que se está lidiando con un tema que ha sido escasamente estudiado con anterioridad en la literatura, la atención se centra en la alternativa de mayor simplicidad. Consecuentemente, se emplea un procedimiento que permite establecer una conexión entre simulaciones de diferentes resoluciones numéricas, a través de la cual se pueden inferir propiedades de cantidades físicas por debajo del umbral de resolución en las simulaciones de baja resolución; en un sentido estadístico, evidentemente. Dichas propiedades pueden, entonces, emplearse para poder formar estrellas en dichas simulaciones.

Una vez seleccionada la alternativa de mayor simplicidad, ésta fue implementada en la versión pública del código para simulaciones cosmológicas Arepo, y se corrieron una serie de simulaciones para poder evaluar el grado con el cual dicha alternativa puede superar las dificultades de prescripciones desarrolladas con anterioridad. Los resultados obtenidos son ciertamente prometedores; sin embargo, se requieren de estudios más profundizados que complementen la evaluación en regímenes no considerados en el presente trabajo.

Chapter 1

Introduction

This chapter is intended to provide a description of the context in which the present work is developed and its justification. Accordingly, the purpose and methods of cosmological hydrodynamical simulations are briefly considered, followed by a discussion of the limitations and complications inherent to them as a consequence of their unavoidably finite numerical resolution.

1.1 Cosmological hydrodynamical simulations

Cosmological simulations are intended to assess in a self-consistent manner the large-scale structure and galaxy formation in the Universe by means of computer simulations. To accomplish this, numerical schemes have to be introduced that model all the components of the Universe and their associated physical processes that are cosmologically relevant.

Historically, due to limitations in computational power, the first simulations that were conducted modeled solely the gravitational interaction in a universe composed exclusively of collisionless dark matter (DM), the so-called *N-body* simulations[1], completely neglecting the baryonic component and therefore being unable to be compared directly with observations. Nonetheless, since structure formation in large scales is dominated by DM in the current standard model of cosmology (e.g. Planck Collaboration et al., 2018), these simulations provided valuable insights of the DM distribution in such scales, revealing its web-like structure consisting of voids, walls, filaments and halos, together with insights of the internal structure of these halos as well (Vogelsberger et al., 2020). Furthermore, they allowed for the development of alternative approaches to study galaxy formation and evolution which relied on the post-processing of their output, namely semi-analytical modeling and abundance matching (Somerville and Davé, 2015; Naab and Ostriker, 2017, and references therein).

Over time, with the dramatic increase in computational power, including the hydrodynamics of the cosmic gas in the simulations became possible, hence giving birth to a brand new field of research in computational cosmology: cosmological hydrodynamical simulations. In these simulations, the cosmic gas is modeled as an inviscid ideal gas using the Euler equations of fluid dynamics and the thermodynamics of ideal gases, being immersed in a homogeneously expanding background which is in turn modeled as a spatially flat Friedmann-Lemaître-Robertson-Walker space-time. Euler equations can be formulated in Eulerian, Lagrangian or arbitrary Lagrangian-Eulerian forms, each of them leading to different discretization schemes. These schemes can be further distinguished on the basis of whether or not they employ a mesh to solve the equations, leading to the so-called mesh-based and mesh-free schemes (there are a number of comprehensive reviews in this

[1] A comprehensive review regarding this type of simulations can be found in Bertschinger (1998).

subject, e.g. Somerville and Davé, 2015; Naab and Ostriker, 2017; Vogelsberger et al., 2020).

1.2 Unresolved physical processes

The inclusion of cosmic gas hydrodynamics represents a major, non-trivial achievement in the refinement of cosmological simulations. Nevertheless, there still remains a number of relevant baryonic physical processes that are left unaccounted for, particularly in the kiloparsec scales and below, such as radiative interactions, magnetic fields and nuclear reactions. More importantly, limitations in the attainable numerical resolution currently hinder the correct modeling of the cosmic gas in such scales, thus hindering the modeling of processes impacting galaxy formation and evolution. As a consequence, in order to obtain realistic galaxies using cosmological hydrodynamical simulations, simplified prescriptions have to be introduced that compensate this lack of numerical resolution by modeling the effect of unresolved processes at scales that are marginally resolved in the simulation. Examples of such processes are radiative cooling of the gas, star formation, the formation and growth of supermassive black holes (SMBH), energy feedback into the interstellar medium (ISM) from stars and active galactic nuclei (AGN), and more recently some attention has been devoted to magnetic fields, cosmic rays, radiation fields and dust physics (Vogelsberger et al., 2020).

The introduction of these prescriptions brings about a major inconvenience for cosmological hydrodynamical simulations since, more often than not, it is not possible to arrive at them from first principles given our poor understanding of the related physics and/or the lack of well-established observational constraints. For such cases, then, prescriptions are arrived at following simplified, sometimes phenomenological models which encapsulate the unknown physics in a set of adjustable parameters. The values of these parameters are then set, or *calibrated*, by comparing simulation results to a selection of observed properties of the galaxy population, such as the galaxy stellar mass function (GSMF) and the stellar mass-central black hole mass relation (e.g. Schaye et al., 2015; Pillepich et al., 2018).

1.3 The issue of numerical convergence

Furthermore, whether or not these prescriptions should be setup in such a way as to not require a recalibration when changes to the numerical resolution are made, remains a subject of debate. Such a property is termed *numerical convergence* in the literature (Vogelsberger et al., 2020). Some authors maintain that numerical convergence should always be demanded, arguing that it simplifies the calibration process and allows for a distinction to be made between numerical and physical limitations to the modeling (e.g. Vogelsberger et al., 2013; Pillepich et al., 2018). Nonetheless, numerical convergence constitutes a strict constraint on modeling alternatives, so much so that, in order to achieve it, some rather unphysical strategies are commonly followed. An example of this is the prescription for energy feedback from stars in the previously cited studies. In it, stellar wind is ejected from a star-forming region with a speed that depends on the local DM velocity dispersion, the hydrodynamical interactions of this wind with surrounding gas are disregarded, and it is later absorbed by the nearest gas element once it has traveled far enough from the star-forming region where it originally formed.

Given such state of affairs, other authors choose to relax this constraint and allow for prescriptions that must be calibrated to a particular numerical resolution, otherwise requiring a recalibration (e.g. Crain et al., 2015; Schaye et al., 2015). They argue that, apart from the increased freedom in modeling, such prescriptions lead to a more realistic treatment of marginally resolved phenomena since they can be parameterized with local

hydrodynamical properties of the gas, which are evidently resolution-dependent, allowing them to fully develop their impact on scales that are resolved in the simulation.

In the case of prescriptions for star formation, which are the main subject of the present work, they are inherently resolution-dependent given the constraints imposed on them by observations, as it will be discussed in chapter 3. Furthermore, since these constraints are built on an averaging procedure specific to a particular spatial scale, and given the complex nature of star formation, it is not straightforward to know beforehand the changes they would experience if larger spatial scales are used, and there are indications that such changes are considerable, as it is discussed in section 3.4. Therefore, difficulties modeling star formation in low resolution simulations are twofold: previous prescriptions are inadequate since they have been calibrated to a different numerical resolution, and observational constraints at relevant spatial scales are limited in their applicability. The present work represents an attempt to address these difficulties by studying them, and subsequently proposing and testing a solution.

Chapter 2

Objectives

The following objectives were deemed imperative for the successful conclusion of the present work.

1. To get acquainted with cosmological hydrodynamical simulations through an understanding of their purpose, methods and limitations.

2. To understand the subject of numerical convergence in the context of the prescriptions used to model unresolved physics in these simulations, the primary features affecting it, and the different philosophies that have been adopted hitherto.

3. To understand the theoretical and observational motivations of the current prescriptions employed to model star formation in these simulations and the numerical difficulties bestowed upon them by the necessity to resort to local hydrodynamical properties of the cosmic gas.

4. To formulate a prescription that circumvents the aforementioned difficulty following theoretical, observational and numerical arguments with an emphasis in simplicity of the final proposal.

5. To assess the suitability of the proposal by performing simulations and analyzing the results obtained using widely known properties of the galaxy population in the Universe.

Chapter 3

Star formation

In this chapter, a general overview of star formation is provided, with emphasis being made on star formation laws given their relevance in the prescriptions used to model this phenomenon in cosmological hydrodynamical simulations. A description of some of the most commonly employed prescriptions is likewise included.

3.1 Fundamentals

Even though star formation plays a central role in shaping the Universe as we know it, to date it has remained a poorly understood phenomenon given the wide-range of physical processes affecting it (Krumholz, 2014). The ISM, being composed of ionized, neutral and molecular gas within which chemical reactions take place, unavoidably coupled with radiation and magnetic fields, cosmic rays, gravity, shear and Coriolis forces, and previously formed stars (Mo et al., 2010; Krumholz, 2014), represents a formidable modeling challenge. Star formation inherits this complexity given the fact that it takes place within such a chaotic environment.

Star formation is observed to occur in the dense molecular component of the ISM. Such complexes are frequently termed *molecular clouds* in the literature. As the term suggests, these clouds are distributed in a rather clumpy fashion in the ISM, much like clouds of water vapor in Earth's sky. They are mainly composed of molecular hydrogen and, in the Milky Way, they are observed to exhibit a hierarchical structure in which the largest scale corresponds to the so-called Giant Molecular Clouds (GMC, Mo et al., 2010). GMCs have typical masses around $10^5 - 10^6$ $M_\odot$ and extend over a few tens of parsecs, the corresponding densities being $n_{H_2} \simeq 100 - 500$ cm^{-3}. Additionally, they exhibit a nearly isothermal structure, with temperatures around 10 K (Mo et al., 2010).

Molecular clouds are being permanently bombarded with ionizing and photo-dissociating radiation and cosmic rays, which are mostly absorbed within their outermost layers in a process called *self-shielding*. As consequence, they exhibit a layered structure which, from outside to inside, is composed of ionized, atomic and molecular hydrogen (Krumholz, 2014).

Large-scale cosmological simulations typically have softening lengths of several hundred parsecs (e.g. Vogelsberger et al., 2014; Schaye et al., 2015; Marinacci et al., 2018), and hence their current achievable resolution is still an order of magnitude away from capturing the length scales in which molecular clouds are observed to form. Moreover, they currently lack most of the rich physics that is present in the ISM. Consequently, in order to form stars in these simulations, a prescription is required that establishes the conditions under which collisionless star particles will be spawned from gas elements. Given the complex nature of the ISM, setting up such a prescription is a far-from-trivial modeling task. Fortunately, though, the existence of empirical star formation laws simplifies matters considerably.

3.2 The Kennicutt-Schmidt star formation law

One of the earliest attempts to gain insight of the physical processes affecting star formation consisted in trying to find empirical correlations between the star formation rate (SFR) and thermodynamical properties of the gas in the ISM, both averaged over some suitable length scale. Such correlations are termed *star formation laws* in the literature.

Since observations are restricted to quantities integrated along the line of sight, star formation laws are generally expressed as surface densities; i.e., as quantities per unit pc^2 or kpc^2. However, if a constant scale height is assumed for the ISM, then surface density laws are equivalent to volume density laws. Such an assumption was made by Schmidt (1959), who expressed the volume density of the SFR as a function of the volume density of the ISM gas using a power law,

$$\dot{\rho}_\star \propto \rho_\mathrm{g}^{n_s}, \tag{3.1}$$

and suggested $n_s \sim 2$ by analyzing the distribution of neutral hydrogen and young stars in a direction perpendicular to the Galactic plane. Relationships of this type are commonly referred to as *Schmidt laws* in the literature.

Depending on the length scale that is used to average the quantities and on what constitutes the "gas" in the ISM, several types of Schmidt laws can be defined. For instance, the gas density can be restricted to the contribution from atomic hydrogen, molecular hydrogen or the sum of both (neglecting helium and metals). Furthermore, the averaging can be made over an entire galaxy, leading to the so-called *global* Schmidt laws, or it can be made within a single galaxy averaging over concentric rings (azimuthal averages) or even on a pixel-by-pixel basis, leading in turn to the so-called *local* Schmidt laws (Mo et al., 2010).

Building on the work of Schmidt, Kennicutt (1998b) fitted a global Schmidt law using a sample of normal disk and starburst galaxies, obtaining

$$\dot{\Sigma}_\star = (2.5 \pm 0.7) \times 10^{-4} \left(\frac{\Sigma_\mathrm{g}}{\mathrm{M}_\odot\ \mathrm{pc}^{-2}} \right)^{1.4 \pm 0.15} \mathrm{M}_\odot\ \mathrm{kpc}^{-2}\ \mathrm{yr}^{-1}, \tag{3.2}$$

where Σ_g corresponds to the total (atomic and molecular) gas surface density. Given that Kennicutt used surface densities as opposed to Schmidt's volume densities, Equation 3.2 is typically referred to as a Kennicutt-Schmidt (KS) star formation law. The discussion of global KS laws is deferred to section 4.1 where its usefulness for low resolution simulations is considered. The remainder of the present section will be devoted exclusively to local KS laws, whose sub-galactic spatial scales are suitable for the typical resolutions found in modern large scale cosmological simulations.

With the advent of improved telescopes and instruments, obtaining local laws became possible. Here the discussion is limited to local laws obtained through averaging on a pixel-by-pixel basis, since azimuthal averages typically bin together regions within a galaxy with substantially different local gas and SFR densities, making them inadequate for studying local dependencies between these variables (Schaye and Dalla Vecchia, 2008; Kennicutt and Evans, 2012).

Before discussing local laws, it is useful to introduce a number of definitions that are commonly employed in the literature. Such definitions will be useful as well when discussing star formation prescriptions in the next section. Hence, first is the so-called gas consumption timescale, which quantifies the time it will take to convert the gas within a given region into stars,

$$\tau_\mathrm{SF} \equiv \frac{M_\mathrm{g}}{\dot{M}_\star} \qquad \left(= \frac{\Sigma_\mathrm{g}}{\dot{\Sigma}_\star} = \frac{\rho_\mathrm{g}}{\dot{\rho}_\star} \right). \tag{3.3}$$

Next, the star formation efficiency (SFE) is defined as the ratio of the local free-fall time

to the gas consumption timescale,

$$\epsilon_{\rm SF} \equiv \frac{\tau_{\rm ff}}{\tau_{\rm SF}}, \tag{3.4}$$

the free-fall time $\tau_{\rm ff}$ representing the time required for a uniform, pressure-free sphere to collapse to a point, which can be written as (Mo et al., 2010; Krumholz, 2014)

$$\tau_{\rm ff} = \sqrt{\frac{3\pi}{32G\rho}}, \tag{3.5}$$

where G is the gravitational constant.

Proceeding with local laws, they hold a number of insightful features. First, when considering the SFR as a function of total gas density, a large scatter is found in the index of the power law, ranging from 1 to 3 (Mo et al., 2010). The reason for this is that a sharp decrease in the SFR is observed around surface densities of 10 $\mathrm{M}_\odot$ pc^{-2}, which is typically phrased as there being a *density threshold* for star formation. Second, the SFR is poorly correlated with the density of atomic hydrogen, but in turn is tightly correlated with the density of molecular hydrogen. Third, the surface density of atomic hydrogen is observed to saturate around 10 $\mathrm{M}_\odot$ pc^{-2}, which coincides with the value for the density threshold for star formation. For graphical representations of these features, the reader is referred to Figure 9.4 in Mo et al. (2010), Figure 12 in Kennicutt and Evans (2012), and Figure 2 in Krumholz (2014).

It is now well-established that at surface densities around 10 $\mathrm{M}_\odot$ pc^{-2} a phase transition takes place in the ISM, whereby hydrogen atoms combine to form molecules (Schaye and Dalla Vecchia, 2008; Mo et al., 2010; Kennicutt and Evans, 2012; Krumholz, 2014), although this value may depend on metallicity (Krumholz, 2014). Furthermore, there are several possible explanations for the tight correlation between SFR and the density of molecular hydrogen (Schaye, 2004; Mo et al., 2010; Krumholz, 2014), but consensus has yet to be reached.

Another relevant point regarding local laws is that the gas consumption timescale appears to be constant for gas densities outside the region where the phase transition takes place; or equivalently, the index of the KS law is found to be around unity in such regions. The values of this timescale, though, for the regions above and below the threshold, differ by a factor of 50, being around 2 and 100 Gyr respectively (Krumholz, 2014). For the former region, the same study reports that data are consistent with a universal SFE of $\epsilon_{\rm SF} \simeq 0.01$, meaning that in molecular clouds the gas consumption timescale is greater than their free-fall time by a factor of 100. The physical processes behind such an inefficient star formation remain a subject of debate in the community.

As it can be seen, despite the fact that local star formation laws entail an averaging procedure over length scales of the order of kiloparsecs, they provide valuable insights into the properties of star formation, motivating the formulation of a wide range of theories to explain them. Furthermore, considering that a self-consistent picture of star formation has yet to emerge, they constitute the sole kiloparsec-scale constraint on star formation prescriptions introduced to cosmological simulations, which are themselves calibrated specifically to reproduce these laws, as will be discussed in the next section.

3.3 Prescriptions to model star formation

Modeling star formation in cosmological hydrodynamical simulations was pioneered by Katz (1992). In it, a prescription was introduced in which a Schmidt law was employed to quantify the rate of stellar mass production in gas elements that satisfied a specific set of criteria to be considered star-forming. Then, a probability of spawning a star particle from a gas element was calculated based on the ratio of the amount of stellar

mass produced during a time step to the mass of the gas element. Amazingly enough, this algorithm for star formation is largely preserved in modern prescriptions, with some modifications introduced owing to improvements in the understanding of both the physics of star formation and the numerical performance of the algorithm, as will be discussed in this section.

Keeping in mind the objectives of the present work, attention will be focused on prescriptions that have been used in large scale cosmological hydrodynamical simulations. Hence, referring to the compilation of such simulations made by Vogelsberger et al. (2020), three prescriptions emerge: Springel and Hernquist (2003), Schaye and Dalla Vecchia (2008) and Krumholz et al. (2009).

Nevertheless, the prescription of Krumholz et al. (2009) will be excluded from this discussion for the following reason. In it, the SFR is expressed as a function of the density of molecular hydrogen within a gas element, the latter being approximated using a parameterization of the fraction of molecular gas within a cloud in the ISM with metallicity and average density. Regarding this course of action, Naab and Ostriker (2017) argue that it increases the complexity and uncertainty of the prescription considering that the molecular fraction of a cloud depends on a wide-range of physical processes which are unresolved in cosmological simulations. Further, they add that it remains unclear whether the formation of molecular hydrogen is the main driver of star formation, a view that is shared by, e.g., Elmegreen (2018).

3.3.1 Springel & Hernquist

The prescription of Springel and Hernquist (2003) models each gas element as being composed of hot and cold phases, much like the molecular complexes observed in the ISM. It assumes that an averaging procedure is available such that, on the one hand, these phases can be described solely by their average density and internal energy, and on the other hand, it enables physical processes to be introduced that can be formulated in terms of these average quantities, and through which said phases can exchange mass and internal energy.

In such a framework, the densities and internal energies of the phases within each gas element can be tracked by writing a set of simple differential equations for their time evolution, taking into account the physical processes introduced (equations (5-6) and (8-9) in Springel and Hernquist, 2003). The cold phase temperature is assumed to have a constant value of $T_c \simeq 10^3$ K, which leads to a constant internal energy u_c for this phase, thereby reducing by one the number of differential equations to be solved. Furthermore, the hydrodynamic interactions are followed only for the hot phase gas, while the cold phase interacts only through gravity.

Stars are allowed to form from the cold phase at a rate that is inferred from Equations 3.3 and 3.4,

$$\dot{\rho}_\star = (1-\beta)\,\frac{\rho_c}{\tau_{\rm SF}} = (1-\beta)\,\epsilon_{\rm SF}\frac{\rho_c}{\tau_{\rm ff}}, \tag{3.6}$$

where the factor $1-\beta$ comes from the assumption that a mass fraction β of the stars formed instantly explode as core-collapse supernovae, the value of this mass fraction depending on the choice of the initial mass function (IMF). Taking into account Equation 3.5 for the free-fall time, this last expression is equivalent to a KS law with index 1.5[1], which is at odds with index values of ∼1.4 and ∼1.0 found for empirical local KS laws[2], as discussed in the previous section. Given this difference, a new fit has to be performed to the data from Kennicutt (1998b) and forcing the index of the power law to a value of 1.5. Then,

[1] Provided a constant scale height is assumed throughout the disk of a galaxy.

[2] An index of ∼1.4 is obtained from azimuthal averages of the data, while an index of ∼1.0 from pixel-by-pixel averages (Kennicutt and Evans, 2012; Krumholz, 2014).

the output from simulations are made to replicate this tailored KS law by calibrating the value of $\epsilon_{\rm SF}$.

The physical processes introduced in the model that entail mass and internal energy exchange between phases are the following. Cold phase gas, as mentioned earlier, is allowed to lose mass to stars at a rate of $\rho_c/\tau_{\rm SF}$, of which a fraction $1-\beta$ goes into stars and the remaining fraction β that explodes as supernovae is deposited into the hot phase gas, thereby increasing its internal energy. Moreover, cold phase gas is allowed to "evaporate" to the hot phase as a consequence of supernova explosions that are present when star formation is taking place.

The processes within the hot phase gas, however, are made to depend on the regime in which the gas element containing it is found. Two regimes are distinguished, depending on whether the density of the gas element is above or below a specified threshold, $\rho_{\rm th}$. In the latter case, the hot phase solely looses internal energy through an optically thin radiative cooling prescription. In the former case, the hot phase is assumed to be thermally unstable, and consequently "condenses" to the cold phase, thereby increasing the density of the latter and favoring star formation.

In this way, the overall effect of this prescription is to regulate the temperature and pressure of gas elements in which star formation is taking place. This can be seen as follows. Consider a gas element for which $\rho_c = 0$; i.e., it is composed solely of a hot phase. If its density is such that $\rho \leq \rho_{\rm th}$, then the only effect this prescription will have in it is the radiative cooling. Now suppose that this gas element manages to cool sufficiently so that $\rho > \rho_{\rm th}$, then this gas element enters the thermally unstable regime and the hot phase is allowed to condense, thereby bringing into existence a cold phase within the gas element. The latter will trigger the formation of a star particle of a given mass, a fraction of which will immediately explode as a supernova, with the subsequent increase in the internal energy of the hot phase gas. This will manifest itself as an increase in temperature and pressure in the gas element, the latter being given by $P = (\gamma - 1)\,(\rho_h u_h + \rho_c u_c)$, where the quantity $\rho_h u_h + \rho_c u_c$ is the internal energy per unit volume of the gas element.

In the literature, the effect just described is phrased as the prescription introducing an *effective equation of state* (eEOS) for gas elements in which star formation is taking place. Such an eEOS is required in the numerical scheme in order to prevent gas elements from undergoing catastrophic cooling once they reach a sufficiently high density, which was one of the most important difficulties cosmological hydrodynamical simulations had to overcome at their early stages (Somerville and Davé, 2015; Naab and Ostriker, 2017).

3.3.2 Schaye & Dalla Vecchia

The prescription of Schaye and Dalla Vecchia (2008) follows a substantially different and simpler approach to model star formation when compared to the previous one.

Firstly, an analytical connection is established between surface and volume densities which does not require the assumption of a constant scale height throughout the disk of a galaxy. It is based, in turn, on the assumption that the disk is self-gravitating, as originally suggested in Schaye (2001), which enables to approximate the local scale height with the local Jeans length. The latter is given by

$$\lambda_{\rm J} \equiv \frac{c_s}{(G\rho)^{1/2}},$$

where c_s is the *effective* speed of sound (including turbulent pressure) and ρ represents the combined local density of gas and stars. Writing the latter as $\rho = \rho_{\rm g}/f_{\rm g}$, where $f_{\rm g}$ is the local gas fraction, and $c_s^2 = \gamma P_{\rm tot}/\rho_{\rm g}$, this last equation can be written as

$$\lambda_{\rm J} = \frac{1}{\rho_{\rm g}} \left(\frac{\gamma\, f_{\rm g} P_{\rm tot}}{G} \right)^{1/2}.$$

Hence, the gas surface density can be approximated as

$$\Sigma_{\rm g} = \lambda_{\rm J}\rho_{\rm g} = \left(\frac{\gamma}{G}\right)^{1/2} (f_{\rm g}\, P_{\rm tot})^{1/2}\,. \tag{3.7}$$

Using this relation and a KS law, the SFR can be written as a function of total pressure in the gas. Noticing that

$$\frac{\Sigma_{\rm g}}{\dot{\Sigma}_\star} = \frac{m_{\rm g}}{\dot{m}_\star},$$

the following is obtained

$$\dot{m}_\star = m_g\, A \left(\frac{\gamma}{G}\, f_{\rm g}\, P_{\rm tot}\right)^{(n-1)/2}, \tag{3.8}$$

where A and n are the normalization and index of the KS law, respectively. Equations 3.7 and 3.8 open the possibility of expressing the SFR and its density threshold as a function of total gas pressure, using as input an empirical KS law and without requiring the calibration of a single free parameter. Furthermore, they predict that in the cases where the SFR is written as a function of volume densities; i.e., when a Schmidt law is assumed, its index is different from the index of the empirical KS law, this difference depending on the index of the assumed eEOS (eq. (15) or (16) in Schaye and Dalla Vecchia, 2008). This is particularly problematic for the prescription of Springel and Hernquist (2003) described in the previous section, considering that the index of its eEOS is not constant, but actually a function of gas density[3]. Moreover, this problem is not present when the SFR is written as a function of total gas pressure.

This last statement leads to the main advantage of this prescription. It means that the empirical KS law will be reproduced by the simulation regardless of the choice of eEOS, hence giving the freedom of selecting the latter to accomplish different purposes. For example, Schaye and Dalla Vecchia recommend a polytropic eEOS with index 4/3 since this leads to a Jeans mass of the gas elements that is independent of their density. The same holds for the ratio of the Jeans length to the spatial resolution of the numerical scheme for the hydrodynamics. They argue that such properties guarantee that both Jeans mass and length of gas elements are resolved in the simulation regardless of the their density, preventing the development of known numerical inaccuracies when these conditions are not met.

3.4 Caveats related to star formation laws

As discussed in previous sections, prescriptions to model star formation make use of star formation laws to constrain their behavior at marginally resolved scales. Building on this discussion, the present section aims to assess the observational uncertainties and numerical inconveniences brought about by the use of such laws.

3.4.1 Systematic uncertainties

Obtaining star formation laws requires measurements of SFRs and masses of the different components of the ISM, which unavoidably carry uncertainties with them.

The SFR is inferred by measuring the radiation emitted by young stars. This relies on the reasonable notion that the population of such stars is indicative of the star formation that took place in the recent past, in a specific region. A number of wavelength bands

[3]For the case of said prescription, this means that star-forming regions of different densities are fitting different KS laws.

or spectral lines can be used for this purpose, each of them being related to the emission of young stars through various physical mechanisms. For instance, near-ultraviolet (UV) continuum emission is dominated by young stars according to synthetic stellar population models, the Hα line is expected to be excited in atomic gas surrounding young stars, and far-infrared (FIR) continuum is expected when dust particles are heated by preferentially absorbing UV light emitted from young stars (Kennicutt, 1998a; Kennicutt and Evans, 2012). These are termed *diagnostic methods* in the literature, and their connection with the population of young stars is established through synthetic stellar population models, which require the assumption of age distribution, chemical composition and IMF of the underlying stellar population (Kennicutt and Evans, 2012), and enable *calibrations* to be developed that relate measured luminosities of diagnostic methods to integrated SFRs (Kennicutt, 1998a; Kennicutt and Evans, 2012).

Hence, uncertainties in the determination of SFRs have contributions from measuring luminosities of diagnostic methods and the uncertainties inherent to synthetic stellar population models. For the former, dust attenuation impairs UV and Hα measurements, while the lack thereof in turn impairs FIR and radio measurements, in all cases possibly leading to underestimation or overestimation of the SFR, depending on the properties of the surrounding medium (Kennicutt and Evans, 2012). As for the latter, synthetic stellar population models are known to be sensitive to metallicity and the choice of IMF (Kennicutt and Evans, 2012).

For the case of the ISM, typically masses are obtained for atomic and molecular hydrogen, and the so-called *dense gas*. Different spectral lines (or *gas tracers*) are used for each of these components. Cold atomic hydrogen ($T \lesssim 70$ K) is traced by its 21 cm hyperfine transition, molecular hydrogen (the most abundant molecule in the ISM) by the $J = 1 \rightarrow 0$ transition of the CO molecule, while dense gas ($n > 10^4$ cm^{-3}) by transitions akin to the latter but from the CS and HCN molecules (Kennicutt and Evans, 2012). Masses are obtained by means of expressions that relate them to line intensities and other parameters (Kennicutt and Evans, 2012).

Hence, uncertainties in mass determination are similar to the case of the SFR with respect to the measurement of line intensities. Notwithstanding this, their largest source of uncertainty stem from the relationships between masses and line intensities employed, within which the case of the CO molecule is the most widely known (Kennicutt and Evans, 2012). In it, line intensity is converted to column density of molecular hydrogen through a factor denoted as $X(CO)$. This factor has poorly understood dependencies with metallicity, gas density and temperature (Kennicutt and Evans, 2012; Bolatto et al., 2013), and such is the state of affairs regarding it that, for the case of extragalactic measurements, even fixing metallicity to solar values leads to uncertainties of a factor of two (Bolatto et al., 2013), which translate to same order uncertainties in the inferred mass of molecular hydrogen.

Given the variety of measurements that can be used to obtain SFRs and gas masses, in addition to the aforementioned uncertainties related to them, the large scatter observed in star formation laws should not be surprising (e.g. Kennicutt and Evans, 2012; Orr et al., 2018; Williams et al., 2018; Murphy et al., 2019, and references therein), particularly in sub-kiloparsec scales, so much so that it has motivated a number of studies that suggest the breakdown of the KS law at such scales (e.g. Calzetti et al., 2012; Feldmann et al., 2012; Kruijssen and Longmore, 2014; Khoperskov and Vasiliev, 2017).

3.4.2 Numerical convergence in prescriptions

From the numerical perspective, the reliance of star formation prescriptions on star formation laws is troublesome for their numerical convergence properties, the impact being twofold.

First, it requires the SFR to be expressed as a function of local hydrodynamical properties of the gas elements, such as density or pressure, which are evidently influenced by changes in numerical resolution. Furthermore, KS laws which relate the SFR to *total* gas density or pressure must be used, since simulations do not track the molecular component within gas elements, and for good reasons (as it was discussed in section 3.3). This means that the commonly observed phase transition around $\Sigma_g = 10\ M_\odot\ pc^{-2}$ has to be accounted for, which is typically achieved through a volume density threshold for star formation, as it is done in the prescriptions discussed in section 3.3, thereby introducing another dependence on a local hydrodynamical property.

Second, star formation laws are themselves highly dependent on the spatial scale used to average the observed quantities (e.g. Williams et al., 2018); hence, for modeling purposes, a particular version of such laws is adequate only within a certain range of numerical resolution of the target simulation, which should be chosen such that the softening lengths in the latter are comparable to the aforementioned spatial scales.

Chapter 4

Methodology

The previous chapters aimed at covering the astrophysical baggage required to develop a prescription to model star formation in low resolution cosmological hydrodynamical simulations. Having achieved that, the avenues selected to pursuit this goal and their subsequent development ought to be described. Hence, this chapter first brings attention to global KS laws as a valuable resource in the present circumstances. Following this, a slight digression is made to introduce the simulations that were run which constituted the means used to achieve this goal. Next, the strategy adopted and the methods devised in accordance with said strategy are first broadly outlined, and then a detailed account of their development is provided. This entire process, due to extension restrictions, yields a single candidate method, which then proceeds to the assessment phase that is described in the following chapter.

For clarity, previous prescriptions developed for higher resolution simulations (i.e., those that were described in section 3.3) will be henceforth referred to as *standard* prescriptions.

4.1 The case for a global Kennicutt-Schmidt law

The coarser, galactic scales of global KS laws which, contrary to local laws, more closely resemble the softening lengths of low resolution cosmological hydrodynamical simulations (Table 4.1), justifies their consideration in the quest for a prescription to model star formation in these simulations.

Global KS laws are obtained by quantifying the total gas mass and total SFR of galaxies using one of the methods described in the previous section, dividing them by the area of the star-forming disk of the corresponding galaxy, and fitting the results to a power law (Kennicutt and Evans, 2012). The observed index of the power law is $1.4-1.5$ when a single value for $X(CO)$ is assumed for all the galaxies considered (Kennicutt and Evans, 2012), although this is hardly an appropriate assumption given the known dependencies of this factor, as discussed in section 3.4. Hence, there is considerable uncertainty in the value of this index (Kennicutt and Evans, 2012).

The introduction of a global KS law into a star formation prescription would require essentially the same procedure as the case of local laws. For instance, they would have to be cast in a form that is manageable for simulations; i.e., using volume densities or total pressures. However, a drawback emerges at this point which originates from the known difficulty of defining the boundaries of a galaxy, which is likely the reason behind the choice of using the area of the star-forming disk to compute surface densities in global KS laws. This means that these laws relate SFR and gas mass only within the star-forming portion of galaxies. Consequently, a diligent implementation of them into a star formation prescription requires a companion function that enables the determination of the fraction

of a gas element that is forming stars. Such a function essentially has the task of predicting the internal structure of a gas element using as input the averaged properties of the same and surrounding gas elements, since more detailed information within simulations is not available. Hence, to make this prediction possible, the required additional information would have to come from sources outside the corresponding simulation.

Nonetheless, no further drawbacks should be expected in this implementation since, as mentioned earlier, the procedure should be essentially the same as for local laws. Therefore, global KS laws deserve full consideration as a potential means to achieve the objectives of the present work.

4.2 The simulations run

Anticipating subsequent discussions, in this section a slight digression is made to describe the simulations run for the purposes of the present work. They will be distinguished as *fiducial*, *control* and *calibration* simulations.

The fiducial simulation was considered the reference, or benchmark, simulation to which the others were compared to and/or had to reproduce. The justification for this is that its numerical resolution was chosen so as to be comparable to the resolution of previously run large scale cosmological hydrodynamical simulations (e.g. Schaye et al., 2015; Marinacci et al., 2018) and it used a standard prescription for star formation; consequently, this simulation was run in a regime where both the code and the standard prescription are known to be well-behaved. Moveover, the control simulation had the same setup as the fiducial simulation, the sole distinction being its lower numerical resolution. Its purpose was to enable the assessment, on the one hand, of the impact of this lower resolution on the results of the fiducial simulation and, on the other hand, of the improvement achieved with the prescription developed in this work. Finally, the calibration simulations had the same numerical resolution as the control simulation, and in them the standard prescription for star formation was replaced by the prescription developed in this work. Their purpose was to enable the calibration of the free parameters in the foregoing prescription. Table 4.1 summarizes the characteristics of all the simulations run. It should be mentioned that a computational box of 20 Mpc on each side was chosen so as to require modest computational resources for running the simulations.

A depiction of the effects of changes in numerical resolution is shown in Figure 4.1, where the images comprise a projection of size 9×16 Mpc in (a) the fiducial simulation, (b) an intermediate resolution simulation included for illustrative purposes and (c) the control simulation. The images were created using the Splotch[1] software package. The role played by numerical resolution in revealing structure in ever smaller spatial scales, and the smoothing effect that its reduction entails for the physical properties in simulations, are clearly seen in Figure 4.1.

All simulations were run in the LaPalma Supercomputer, located at the Instituto de Astrofísica de Canarias. The public version of the Arepo code (Springel, 2010; Weinberger et al., 2019) was used, which implements the star formation prescription from Springel and Hernquist (2003) and a radiative cooling prescription. It does not include any additional prescriptions; nonetheless, this turns out to be convenient for the purposes of the present work for the reasons that are indicated in section 5.1.

[1] http://www.mpa-garching.mpg.de/~kdolag/Splotch

Table 4.1: (a) Parameters common to all simulations and (b) their distinctive characteristics. In the former, L is the side of the computational box in comoving Mpc (cMpc); $\Omega_{\rm m}$, $\Omega_{\rm b}$ and Ω_Λ are the average densities of matter, baryons, dark energy in units of the critical density at redshift zero; and h is the Hubble parameter. In the latter, the columns show the simulations' names, number of resolution elements, initial mass of gas elements, mass of DM particles, softening lengths in comoving kpc (ckpc) and the star formation prescription.

(a)

Parameter	Value
L, cMpc	20
$\Omega_{\rm m}$	0.25
$\Omega_{\rm b}$	0.04
Ω_Λ	0.75
h	0.7

(b)

Simulation	N	$m_{\rm g}$, $\rm M_\odot$	$m_{\rm dm}$, $\rm M_\odot$	ϵ, ckpc	SF prescr.
Fiducial	288^3	1.82×10^6	1.14×10^7	2.8	Standard
Control	72^3	1.17×10^8	7.29×10^8	11.2	Standard
Calibration	72^3	1.17×10^8	7.29×10^8	11.2	This work

4.3 Arriving at a prescription for star formation

4.3.1 Constraining the avenues to be considered

There are presumably a number of different approaches, theoretical and/or empirical, that could be followed to arrive at a prescription for star formation at low numerical resolution, perhaps encompassing a wide range in degrees of sophistication. The present

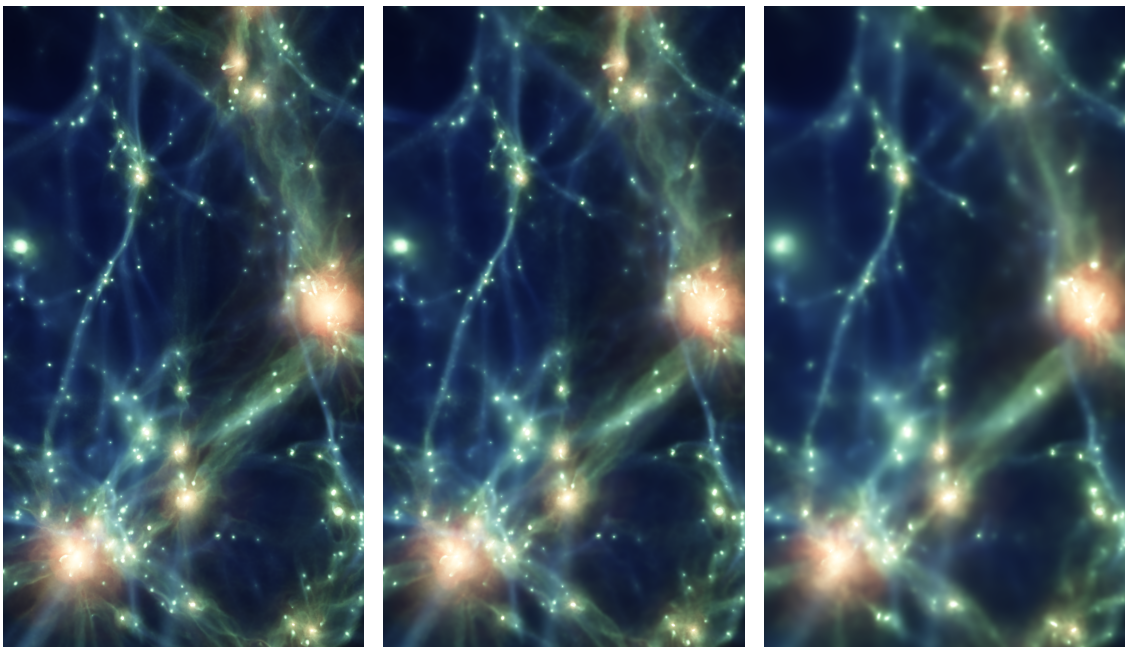

(a) (b) (c)

Figure 4.1: A visualization of some of the simulations run in the present work. The images comprise a projected view of 9×16 cMpc at redshift zero of the computational box in (a) the fiducial simulation, (b) an intermediate resolution simulation included for illustrative purposes and (c) the control simulation. From left to right, numerical resolution decreases by factors of eight. Intensity denotes gas density and colors denote gas temperature, both in logarithmic scale. Created using the Splotch software package (the reference can be found in the text).

work, however, focused in a straightforward approach that consisted in attempting to "generalize", so to speak, standard prescriptions. What is meant by this is that the main framework of these prescriptions were retained, and attention was focused in making adjustments in the way the SFR is determined. The rationale behind this choice is to minimize the potential unintended consequences of substantially modifying well-tested and well-behaved prescriptions, which could negatively impact the numerical stability and/or accuracy of the code.

Accordingly, two methods were devised to accomplish this, which will henceforth be referred to as **Method I** and **Method II**. An outline of each of them follows, and a detailed account of their development is deferred to subsection 4.3.2.

Method I On the basis of the discussion in section 4.1, this method consists in attempting to substitute the local KS law used in standard prescriptions with a global KS law. The drawback related to such an approach, as identified in the foregoing section, can be addressed by **(1)** establishing a set of criteria through which gas elements can be distinguished between ordinary or star-forming and **(2)** using high resolution simulations to analyze the distribution of star-forming gas at spatial scales that are relevant for low resolution simulations. This analysis is expected to yield a relationship between the fraction of a gas element that is forming stars and its averaged properties, like density or pressure. If this is achieved, then using this fraction a global KS law yields the SFR of the gas element, and the unmodified portion of the standard prescription would lead to the spawning of star particles using this SFR.

Method II Alternatively, rather than attempting to determine the fraction of gas elements that is forming stars and using it to calculate SFRs, a simpler approach consists of leapfrogging this step and attempt to find a direct relationship between the SFR and averaged properties of gas elements. This eliminates the requirement of distinguishing between ordinary and star-forming gas elements, thus leading, if attainable, to a cleaner prescription. Having obtained such a relationship, the procedure to spawn star particles would be analogous to the one described for Method I.

4.3.2 Developing the alternatives

This subsection describes in detail the series of steps followed in the attempt of realizing the methods outlined in the previous subsection. Arguably complicating the discussion, the choice was made to respect the chronological order in which the original developments were made, thus emphasizing the trial-and-error nature of this process.

Method I

Recapitulating, this method attempts to substitute a local KS law with a global KS law as the means of relating SFRs and densities of gas elements in star formation prescriptions. A complication arises due to the fact that a global KS law relates these quantities solely for the fraction of gas elements that is forming stars. Consequently, in order for a global KS law to serve its intended purpose in a prescription, this fraction needs to be determined.

To accomplish this, the fiducial simulation was used (section 4.2). The rationale behind this approach is the notion that a connection can be made between simulations of different resolutions, whereby a higher resolution simulation can be used to determine, on average, the internal distribution of properties in gas elements of a lower resolution simulation. In practice, this is achieved through a statistical analysis of the distribution of gas elements and their properties in the higher resolution simulation, coupled with a smoothing procedure that establishes a connection with less resolved structures in lower

resolution simulations. Following this approach, two possible alternatives were contemplated to determine the fraction of a gas element that is forming stars, which are described in the following paragraphs.

If the gas density probability density function (PDF), $\mathcal{P}(\rho_{\rm g}; \bar{\mathbf{x}})$, can be parameterized with quantities $\bar{\mathbf{x}}$ averaged over a suitable spatial scale, and if star-forming gas is taken as the gas which has a density above a specified threshold $\rho_{\rm g,th}$, then the fraction of star-forming gas would be simply given by $\mathcal{P}(\rho_{\rm g} > \rho_{\rm g,th} \,|\, \bar{\mathbf{x}})$. Furthermore, the number of averaged properties used to parameterize this PDF must be kept to a minimum given that a simple prescription is desired. Hence, on the basis of physical considerations, it was deemed appropriate to use gas density and redshift for this parameterization, so that $\mathcal{P}(\rho_{\rm g}; \bar{\rho}_{\rm g}, z)$.

This PDF was obtained empirically using the output from the fiducial simulation and resorting to the following procedure. The computational box was divided in a Cartesian grid in such a way that the average baryonic mass contained in each of the cells of the grid matched the mass of gas elements in the target low resolution simulation[2]. Then, for each of the cells, their average gas density was calculated, together with their gas density PDF. Finally, the cells were binned according to their average gas density, and a representative average gas density and PDF were determined for each bin. Carrying out this procedure for every snapshot[3] of the fiducial simulation yields a collection of sample points of the desired PDF. Figure 4.2 shows the results that are obtained.

The next step would consist of introducing a sampling scheme for this PDF in order to obtain $\mathcal{P}(\rho_{\rm g} > \rho_{\rm g,th} \,|\, \bar{\rho}_{\rm g}, z)$. However, at this stage it was recognized that a more straightforward alternative would be to directly parameterize the mass fraction of a gas element that is forming stars, since this avoids the need to sample the PDF. Hence, attention was diverted into this new alternative.

The procedure to obtain the foregoing mass fraction is similar to the previously followed for the gas density PDF. The computational box of the fiducial simulation is still divided with a Cartesian grid and the average density is calculated for each cell. In this case, however, the mass of gas elements that are forming stars[4] is distributed to surrounding

[2] Which, in the present work, corresponds to the calibration simulations (section 4.2).
[3] That is, the bulk of the output of a simulation for a given redshift.
[4] Which are still taken as the gas elements whose density is above a specified threshold.

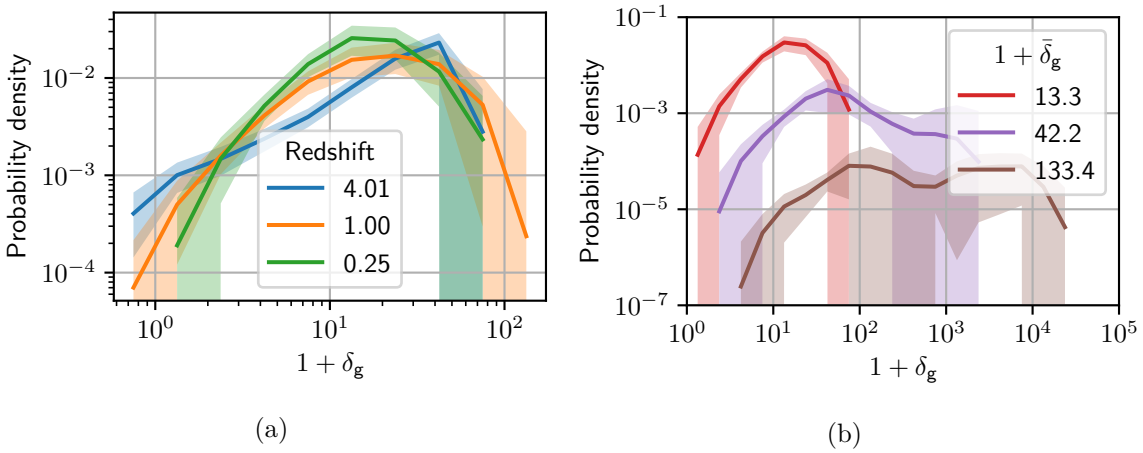

Figure 4.2: The PDF $\mathcal{P}(\rho_{\rm g}; \bar{\rho}_{\rm g}, z)$ obtained empirically using the fiducial simulation, where $\rho_{\rm g}$ and $\bar{\rho}_{\rm g}$ are written as $1+\delta_{\rm g}$ and $1+\bar{\delta}_{\rm g}$, respectively. $\delta_{\rm g}$ is the overdensity of gas elements with respect to the average baryonic density at redshift zero. Slices of $\mathcal{P}(\rho_{\rm g}; \bar{\rho}_{\rm g}, z)$ are shown for (a) $1+\bar{\delta}_{\rm g} = 13.3$ and (b) $z = 0$, with additional slices shown in the legends. Shaded regions indicate the interquartile range.

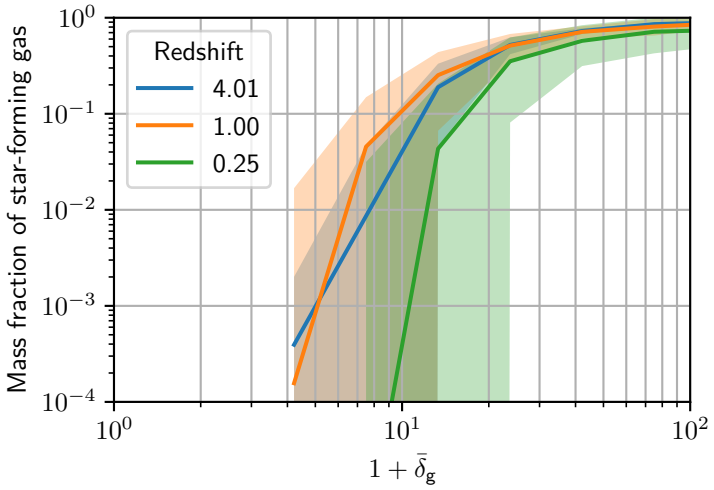

Figure 4.3: The mass fraction of a gas element that is star-forming as a function of its density, at three redshifts. Shaded regions indicate the interquartile range. $\bar{\delta}_g$ is the overdensity of gas elements with respect to the average baryonic density at redshift zero.

cells using the cloud-in-cell (CIC) method. Then, this accumulated mass of star-forming gas is normalized by the total gas mass (i.e., ordinary and star-forming) that each cell contains, and likewise the cells are binned according to their average gas density, with a representative average gas density and mass fraction being determined for each bin. Figure 4.3 shows the results obtained with this alternative for a number of redshifts.

Given the distribution of the obtained points, as seen in Figure 4.3, an analytical fit could be attempted. The combination of such a fit with a global KS law, hence, effectively supersedes a local KS law in its role of relating SFRs and gas densities in a simulation.

Even though both of the alternatives contemplated to implement this Method I could certainly lead to a successful prescription, attention was diverted again to an even simpler approach, which is the one referred to as Method II in subsection 4.3.1 and is discussed next.

Method II

In this method, the attempt was made to directly parameterize the SFR with the density of gas elements and redshift, following an approach similar to the one used in Method I. Since the SFR for every star-forming gas element, in units of solar masses per year, is available from the output of the fiducial simulation, it is distributed to the surrounding cells of the grid using the CIC method. Then, again, by binning the cells according to their average gas density, determining a representative average gas density and SFR for each bin, and repeating the same procedure for every snapshot of the fiducial simulation, a collection of points in the SFR-gas density-redshift space are obtained. Figure 4.4 shows the curves outlined by these points for a number of redshifts.

Given the curves observed in Figure 4.4, the simplest expression that reasonably captures the dependencies was considered to be a power law of the form

$$\dot{m}_\star = a\ (1+z)^b \left(1 + \bar{\delta}_g\right)^c, \quad \left[\mathrm{M}_\odot\ \mathrm{yr}^{-1}\right] \tag{4.1}$$

where $\dot{m}_\star$ is the SFR, z is the redshift and $\bar{\delta}_g$ is the overdensity of the gas[5]. The variables denoted by a, b and c constitute free parameters whose values must be set by analyzing the

[5]That is,

$$1 + \bar{\delta}_g = \frac{\bar{\rho}_g}{\Omega_b\, \rho_{c,0}},$$

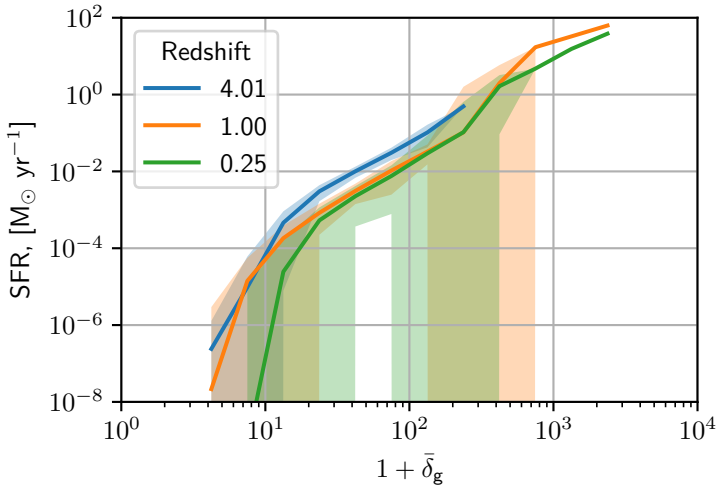

Figure 4.4: The SFR in a gas element as a function of its density, at three redshifts. Shaded regions indicate the interquartile range. $\bar{\delta}_g$ is the overdensity of gas elements with respect to the average baryonic density at redshift zero.

output from simulations in which Equation 4.1 is implemented. This makes the rigorous fitting of these values to the results obtained here unnecessary. In spite of this, a rough estimate is still justified as it serves as a starting point for the calibration process that follows. Hence, by trial-and-error it was found that the values $(a,\, b,\, c) = (10^{-7},\, 1.0,\, 2.5)$ reasonably fit the data. Figure 4.5 shows a couple of such fits, where it can be seen that given the scatter in the results obtained, the values of a, b and c are not well constrained, and hence significant departures from the foregoing values can be expected in the calibration process.

Equation 4.1, then, assumes the role of a local KS law in relating SFR with gas density in a prescription for star formation. Given its simplicity, it constitutes the selected proposal to achieve the goal of the present work, and hence it proceeds to the next phase where its suitability is assessed.

where $\rho_{c,0} = 3H_0^2/8\pi G$ is the critical density of the Universe at redshift zero.

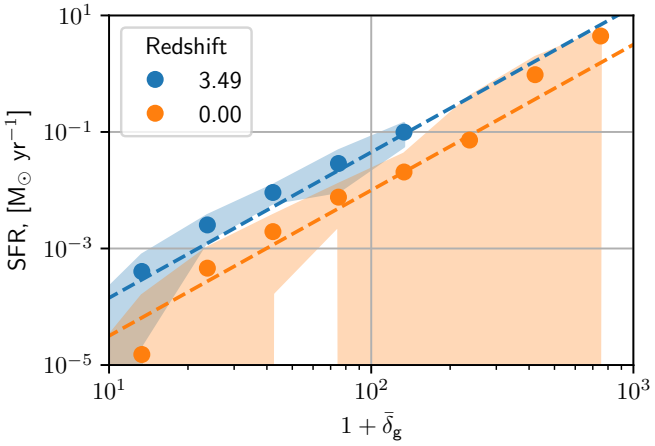

Figure 4.5: Two examples from the approximate fit performed to the results obtained in Method II. Dashed lines correspond to Equation 4.1 using the values $(a,\, b,\, c) = \left(10^{-7},\, 1.0,\, 2.5\right)$. Shaded regions indicate the interquartile range. $\bar{\delta}_g$ is the overdensity of gas elements with respect to the average baryonic density at redshift zero.

Chapter 5

Results

Having reached the stage where a simple prescription has been obtained, what follows is an assessment of the degree to which said prescription can solve the performance issues of standard prescriptions in the low numerical resolution regime. Consequently, the present chapter first discusses the philosophy adopted to execute this assessment considering some limitations that are present, then the calibration process is described and the performance of the best-fitting prescription that was found is analyzed.

5.1 Preliminary remarks

The suitability of prescriptions introduced to cosmological simulations is assessed by comparing simulation results to a number of observables of the galaxy population, the best fit being sought by exploring their parameter space. Ideally, the same procedure should be adopted to perform the assessment of the prescription developed in the present work, however there is an obstacle.

The relatively recent success of large scale cosmological hydrodynamical simulations in reasonably reproducing observations (e.g. Schaye et al., 2015; Marinacci et al., 2018) is predominantly a consequence of the synergy between the prescriptions introduced to them, whereby energy feedback from stars and AGNs play a central role (e.g. Scannapieco et al., 2012). Nonetheless, for the case of low numerical resolution simulations, these prescriptions are not available, thus making any attempt to reproduce observations in the present work futile. Hence, an alternative assessment philosophy had to be introduced.

Considering that the prescription developed aims to address the performance issues of standard prescriptions at low numerical resolution, a straightforward approach to assess the degree to which this is achieved consists in comparing results from simulations having different numerical resolutions, whereby high resolution simulations employ a standard prescription, and those of low resolution, in turn, the prescription developed in the present work. Hence the need for the simulations described in section 4.2.

The comparison is narrowed to a set of widely known relationships of the galaxy population. They were selected in order to enable a reasonable degree of completeness in the assessment by accounting for the distribution of galaxy stellar mass at redshift zero, the time evolution of star formation and the assembly history of galaxies; in other words, the *when*, *where* and *how much* of star formation, in an average sense, were taken into account in the assessment. These relationships are the galaxy stellar mass function (GSMF) at redshift zero, the history of the comoving star formation rate density (SFRD), the history of the comoving stellar mass density (SMD) and the *in situ* fraction of stellar mass (Oser et al., 2010).

In order to obtain the aforementioned relationships, a number of Python scripts were developed through which the outputs of the simulations were processed. The algorithms

needed to accomplish this were mostly straightforward, meaning that there was no room for subjective choices that could impact the results. The exception to this is the determination of the in situ fraction of stellar mass in galaxies. Another slight digression is made here, in order to adequately clarify this issue.

5.1.1 The in situ fraction of stellar mass

The in situ fraction of stellar mass (Oser et al., 2010) refers to the mass fraction of stars in a given galaxy that were born within the virial radius of the galaxies belonging to the *main branch* of said galaxy. The main branch of a given galaxy represents the evolutionary track that contributed the largest mass to its assembly. Alternatively, it is the evolutionary track that is obtained by recursively following the *main progenitors* of said galaxy, the latter referring to the galaxy in a previous time from which the largest fraction of mass in the current galaxy comes from. A much welcomed illustration of these concepts can be found in, e.g., Figure 3 of Somerville and Davé (2015).

The linked list that establishes a connection between all the galaxies in a simulation at every snapshot is known as the *merger tree* said simulation. In order to obtain the in situ mass fraction of galaxies, this merger tree must be determined in order to track the birthplace of their stars. However, the algorithms employed to obtain these merger trees can be quite elaborate (e.g. Jiang et al., 2014); hence, in the present work a simplified algorithm was employed in which the main progenitor of a galaxy was considered to be the one that held the largest fraction of its stars in a previous snapshot, and the main branches were obtained by successively connecting the main progenitors of a subhalo.

In order to assess the degree of agreement between the results obtained with this algorithm and more elaborate ones, the public data release[1] of the IllustrisTNG simulations (Nelson et al., 2019) was used. A comparison was made between the in situ fractions of subhalos at redshift zero obtained using this simplified algorithm and the merger trees available in the foregoing data release. This was performed for the TNG100-3 and TNG300-3 simulations, and Figure 5.1 show the results obtained for the case of the TNG300-3 simulation. In this Figure, both in situ fractions are plotted against each other, and hence the degree of agreement manifests itself as the amount of poits that fall near the line of slope unity. A reasonable agreement can be observed, although some bias is present towards higher in situ fractions in massive galaxies.

Having discussed the necessary remarks, the following section describes the calibration of the free parameters in the prescription developed in the present work.

5.2 Calibrating and assessing the proposed prescription

The calibration was performed by systematically exploring the parameter space of the prescription developed, and selecting the combination of values of (a, b, c) in Equation 4.1 for which the results from the calibration simulations more closely resembled those from the fiducial simulation (section 4.2).

The extent to which the exploration of the parameter space was realized is summarized in Table 5.1. In it, a colored cell indicates a simulation run using the corresponding values of b and c, the red color indicating the starting values of these parameters; i.e., the values obtained with the approximate fit performed to Equation 4.1, as described in section 4.3.2. A total of 28 calibration simulations were run.

Figure 5.2 shows the comparison between the best-fitting calibration simulation with both the fiducial and control simulations. This best-fitting calibration simulation was

[1] https://www.tng-project.org/data/

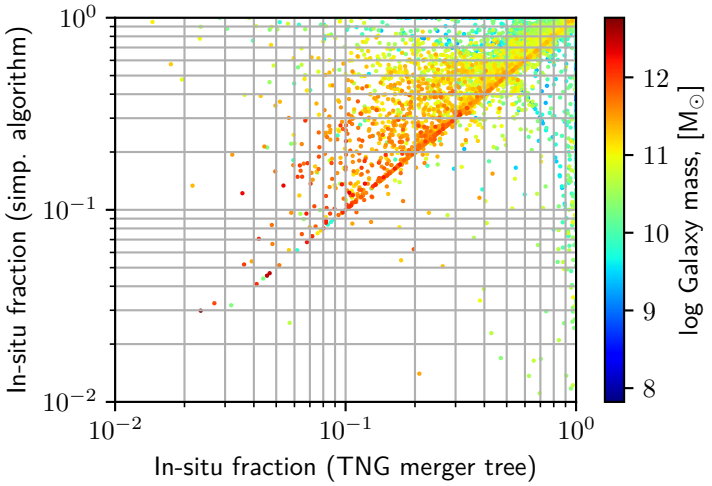

Figure 5.1: In situ stellar mass fractions obtained the simplified algorithm described in the text (vertical axis) and the merger tree available in the public data release of the IllustrisTNG simulations (horizontal axis), plotted against each other for the case of the TNG300-3 simulation.

found for the values $(a,\, b,\, c) = (10^{-7},\, 1.3,\, 1.2)$. It can be seen that the prescription developed in this work succeeds in enabling a calibration simulation to resemble the results of the fiducial simulation with regards to the relationships selected to perform this comparison. The improvement achieved with respect to the control simulation is notable, most importantly for the case of the in situ fraction of stellar mass.

Additional insight can be gained at this point regarding the effects of numerical resolution by looking at both of the plots located at the bottom panel of Figure 5.2. In them, around $z = 6$ a sudden increase in both the SFRD and the SMD are observed in the curve corresponding to the fiducial simulation, a feature that is not captured, however, by neither the control or calibration simulations. This feature is likely caused by the collapse of the most massive structure that can be contained in the simulation box, leading to the formation of high density regions, and consequently to a spike in the formation of stars. Given the lower resolution of the control and calibration simulations, the densities generated by this collapse are not high enough, and the corresponding spike in star formation is completely missed in them.

Table 5.1: A summary of the simulations run exploring the parameter space of the developed prescription, as indicaded by the green cells. The red cell represents the starting values of the parameters. A total of 28 calibration simulations were run.

		b									
		0.50	1.00	1.20	1.25	1.30	1.50	1.75	2.00	2.25	2.50
c	1.00										
	1.15										
	1.20										
	1.25										
	1.30										
	1.50										
	2.00										
	2.50										

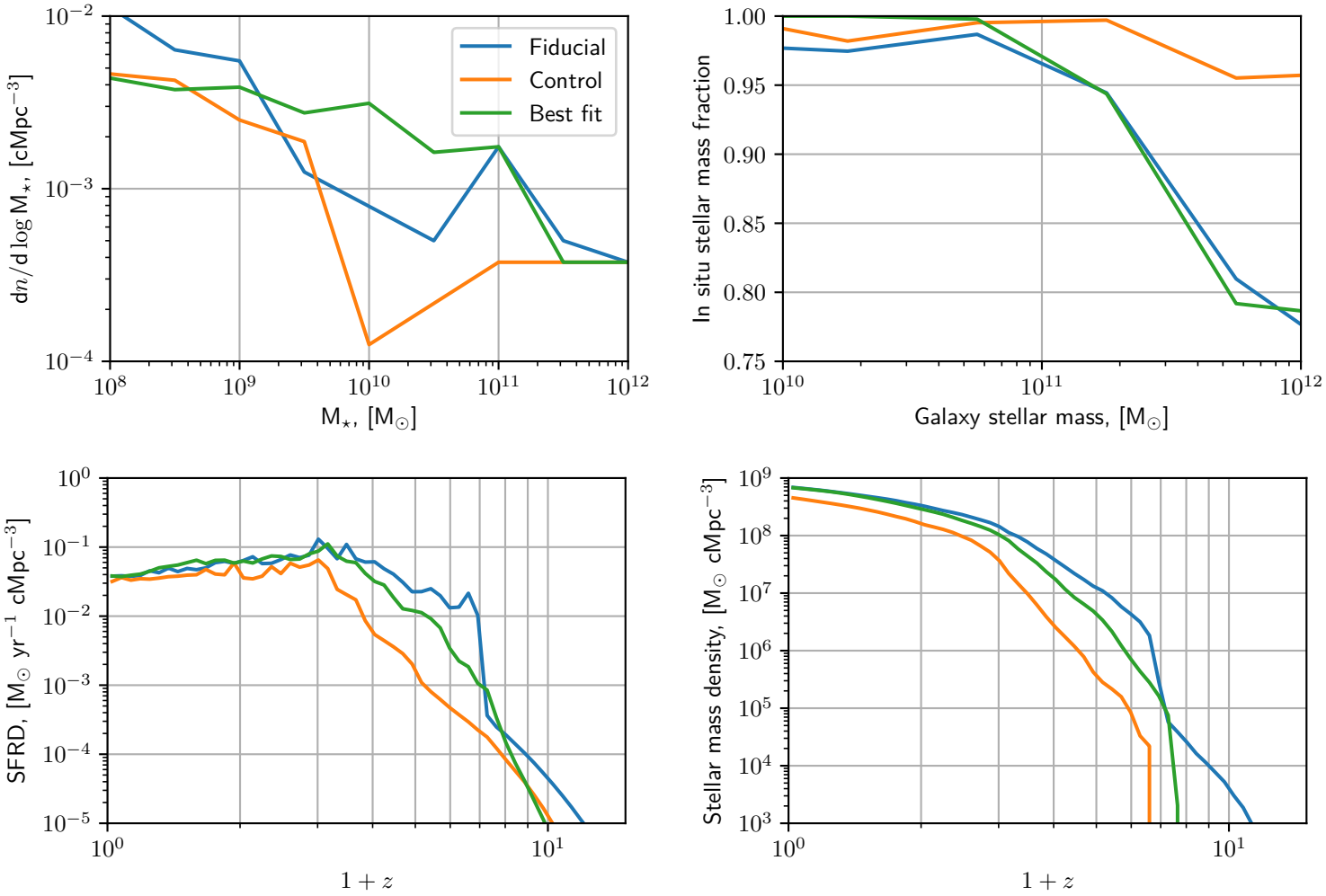

Figure 5.2: Comparison between the fiducial, control and best-fitting calibration simulations. From left to right, top to bottom: GSMF at $z = 0$, in situ mass fraction, comoving SFRD and comoving SMD. The best-fitting calibration simulation corresponds to the values $(a, b, c) = \left(10^{-7}, 1.3, 1.2\right)$ in Equation 4.1.

Chapter 6

Conclusions

The present work aimed at addressing the performance issues of typical prescriptions to model star formation in large scale cosmological hydrodynamical simulations at the low numerical resolution regime. To accomplish this, a careful study of the relevant fields in Astrophysics was made which enabled the acknowledgment that the problem originates in the constraints imposed by star formation laws on the behavior of such prescriptions at marginally resolved spatial scales in the simulations. Since these empirical laws relate star formation rates with local gas properties, such as density or pressure, they inevitably render the prescriptions that resort to them as resolution-dependent. Furthermore, star formation laws themselves suffer substantial modifications when the spatial scales used to average observed quantities are modified. Hence, prescriptions to model star formation in cosmological simulations are considerably and inescapably narrowed in applicability with regards to numerical resolution. Nonetheless, such narrowness has been thus far disregarded in the community, perhaps owing to the fact that star formation laws suffer from significant systematic uncertainties as well, thus making the fine adjustment of its parameters unmerited.

Having acquainted the state of affairs surrounding the problem, a strategy was introduced in order to constraint the number of possible avenues that could be followed to arrive at a solution. The choice was made to focus on the star formation rate calculation of previous prescriptions, leaving the rest of their features unmodified. The rationale for this is that such prescriptions have been extensively tested and their performance is well understood, hence introducing substantial modifications to them is discouraged to prevent the occurrence of ambiguous outcomes.

In accordance with the foregoing strategy, several alternatives were devised and realized. On the basis of their simplicity, a single one of them was selected, which then proceeded to be assessed by exploring the space spanned by its free parameters through low resolution simulations run using a modified version of the Arepo code. The output from such simulations were cast into the form of a number of well-known relationships of the galaxy population, and subsequently compared with analogous results obtained with a higher resolution simulation, which employed a previously developed star formation prescription.

Its was determined that a combination of values for the free parameters of the selected prescription can be found though which the results obtained with the low resolution simulation resemble those obtained with the higher resolution simulation, achieving a considerable improvement over the results that would have been obtained if the former had employed a previously developed star formation prescription.

Nonetheless, this outcome must be celebrated modestly given the limitations of the assessment procedure employed. Firstly, the size of the computational box of the simulations is not adequate to assess the performance of the selected prescription in the high

mass/density regime. For instance, the power law relationship assumed between star formation rate, gas density and redshift may breakdown if sufficient statistics become available at this regime. This lack of statistics likewise impacts the lower mass/density regimes, although to a lesser extent. Secondly, a more in-depth assessment is required to ascertain whether the prescription selected is merely a numerical convenience, or some physical insights can be extracted from it. Thirdly, if this prescription were to hold its performance with further testing, attention should then be diverted into its numerical impact in the different hydrodynamical schemes available, in order to assess the potential spurious effects it introduces. Finally, there are a couple of alternatives that were not given full consideration in the present work, which may as well lead to successful prescriptions for star formation at low numerical resolution. All of this, however, is left to be addressed in future work.

Bibliography

Bertschinger, Edmund. Simulations of Structure Formation in the Universe. *Annual Review of Astron and Astrophys*, 36:599–654, 1998. doi:10.1146/annurev.astro.36.1.599.

Bolatto, Alberto D.; Wolfire, Mark, and Leroy, Adam K. The CO-to-H_2 Conversion Factor. *Annual Review of Astron and Astrophys*, 51(1):207–268, 2013. doi:10.1146/annurev-astro-082812-140944.

Calzetti, D.; Liu, G., and Koda, J. Star Formation Laws: The Effects of Gas Cloud Sampling. *Astrophysical Journal*, 752(2):98, 2012. doi:10.1088/0004-637X/752/2/98.

Crain, Robert A.; Schaye, Joop; Bower, Richard G.; Furlong, Michelle; Schaller, Matthieu; Theuns, Tom; Dalla Vecchia, Claudio; Frenk, Carlos S.; McCarthy, Ian G.; Helly, John C.; Jenkins, Adrian; Rosas-Guevara, Yetli M.; White, Simon D. M., and Trayford, James W. The EAGLE simulations of galaxy formation: calibration of subgrid physics and model variations. *Monthly Notices of the RAS*, 450(2):1937–1961, 2015. doi:10.1093/mnras/stv725.

Elmegreen, Bruce G. On the Appearance of Thresholds in the Dynamical Model of Star Formation. *Astrophysical Journal*, 854(1):16, 2018. doi:10.3847/1538-4357/aaa770.

Feldmann, Robert; Gnedin, Nickolay Y., and Kravtsov, Andrey V. The X-factor in Galaxies. II. The Molecular-hydrogen-Star-formation Relation. *Astrophysical Journal*, 758(2):127, 2012. doi:10.1088/0004-637X/758/2/127.

Jiang, Lilian; Helly, John C.; Cole, Shaun, and Frenk, Carlos S. N-body dark matter haloes with simple hierarchical histories. *Monthly Notices of the RAS*, 440(3):2115–2135, 2014. doi:10.1093/mnras/stu390.

Katz, Neal. Dissipational Galaxy Formation. II. Effects of Star Formation. *Astrophysical Journal*, 391:502, 1992. doi:10.1086/171366.

Kennicutt, Robert C. Star Formation in Galaxies Along the Hubble Sequence. *Annual Review of Astron and Astrophys*, 36:189–232, 1998a. doi:10.1146/annurev.astro.36.1.189.

Kennicutt, Robert C. The Global Schmidt Law in Star-forming Galaxies. *Astrophysical Journal*, 498(2):541–552, 1998b. doi:10.1086/305588.

Kennicutt, Robert C. and Evans, Neal J. Star Formation in the Milky Way and Nearby Galaxies. *Annual Review of Astron and Astrophys*, 50:531–608, 2012. doi:10.1146/annurev-astro-081811-125610.

Khoperskov, Sergey A. and Vasiliev, Evgenii O. A Kennicutt-Schmidt relation at molecular cloud scales and beyond. *Monthly Notices of the RAS*, 468(1):920–926, 2017. doi:10.1093/mnras/stx532.

Kruijssen, J. M. Diederik and Longmore, Steven N. An uncertainty principle for star formation - I. Why galactic star formation relations break down below a certain spatial scale. *Monthly Notices of the RAS*, 439(4):3239–3252, 2014. doi:10.1093/mnras/stu098.

Krumholz, Mark R. The big problems in star formation: The star formation rate, stellar clustering, and the initial mass function. *Physics Reports*, 539:49–134, 2014. doi:10.1016/j.physrep.2014.02.001.

Krumholz, Mark R.; McKee, Christopher F., and Tumlinson, Jason. The Atomic-to-Molecular Transition in Galaxies. II: H I and H_2 Column Densities. *Astrophysical Journal*, 693(1):216–235, 2009. doi:10.1088/0004-637X/693/1/216.

Marinacci, Federico; Vogelsberger, Mark; Pakmor, Rüdiger; Torrey, Paul; Springel, Volker; Hernquist, Lars; Nelson, Dylan; Weinberger, Rainer; Pillepich, Annalisa; Naiman, Jill, and Genel, Shy. First results from the IllustrisTNG simulations: radio haloes and magnetic fields. *Monthly Notices of the RAS*, 480(4):5113–5139, 2018. doi:10.1093/mnras/sty2206.

Mo, Houjun; van den Bosch, Frank C., and White, Simon. *Galaxy Formation and Evolution*. Cambridge University Press, 2010.

Murphy, Eric; Armus, Lee; Bolatto, Alberto; Beswick, Rob; Barcos-Muñoz, Loreto; Brinks, Elias; Condon, James J.; Dale, Daniel A.; Dong, Dillon; Evans, Aaron S.; Kepley, Amanda A.; Leroy, Adam K.; Linden, Sean T.; Madore, Barry F.; Matthews, Allison; Pérez-Torres, Miguel; Schinnerer, Eva; Sargent, Mark T.; Tabatabaei, Fatemeh S.; Turner, Jean L., and Wong, Tony. Towards a Theory for Star Formation on All Scales. *Bulletin of the AAS*, 51(3):523, 2019.

Naab, Thorsten and Ostriker, Jeremiah P. Theoretical Challenges in Galaxy Formation. *Annual Review of Astron and Astrophys*, 55(1):59–109, 2017. doi:10.1146/annurev-astro-081913-040019.

Nelson, Dylan; Springel, Volker; Pillepich, Annalisa; Rodriguez-Gomez, Vicente; Torrey, Paul; Genel, Shy; Vogelsberger, Mark; Pakmor, Ruediger; Marinacci, Federico; Weinberger, Rainer; Kelley, Luke; Lovell, Mark; Diemer, Benedikt, and Hernquist, Lars. The IllustrisTNG simulations: public data release. *Computational Astrophysics and Cosmology*, 6(1):2, 2019. doi:10.1186/s40668-019-0028-x.

Orr, Matthew E.; Hayward, Christopher C.; Hopkins, Philip F.; Chan, T. K.; Faucher-Giguère, Claude-André; Feldmann, Robert; Kereš, Dušan; Murray, Norman, and Quataert, Eliot. What FIREs up star formation: the emergence of the Kennicutt-Schmidt law from feedback. *Monthly Notices of the RAS*, 478(3):3653–3673, 2018. doi:10.1093/mnras/sty1241.

Oser, Ludwig; Ostriker, Jeremiah P.; Naab, Thorsten; Johansson, Peter H., and Burkert, Andreas. The Two Phases of Galaxy Formation. *Astrophysical Journal*, 725(2):2312–2323, 2010. doi:10.1088/0004-637X/725/2/2312.

Pillepich, Annalisa; Springel, Volker; Nelson, Dylan; Genel, Shy; Naiman, Jill; Pakmor, Rüdiger; Hernquist, Lars; Torrey, Paul; Vogelsberger, Mark; Weinberger, Rainer, and Marinacci, Federico. Simulating galaxy formation with the IllustrisTNG model. *Monthly Notices of the RAS*, 473(3):4077–4106, 2018. doi:10.1093/mnras/stx2656.

Planck Collaboration, ; Aghanim, N.; Akrami, Y.; Ashdown, M.; Aumont, J.; Baccigalupi, C.; Ballardini, M.; Banday, A. J.; Barreiro, R. B.; Bartolo, N.; Basak, S.; Battye, R.;

Benabed, K.; Bernard, J. P.; Bersanelli, M.; Bielewicz, P.; Bock, J. J.; Bond, J. R.; Borrill, J.; Bouchet, F. R.; Boulanger, F.; Bucher, M.; Burigana, C.; Butler, R. C.; Calabrese, E.; Cardoso, J. F.; Carron, J.; Challinor, A.; Chiang, H. C.; Chluba, J.; Colombo, L. P. L.; Combet, C.; Contreras, D.; Crill, B. P.; Cuttaia, F.; de Bernardis, P.; de Zotti, G.; Delabrouille, J.; Delouis, J. M.; Di Valentino, E.; Diego, J. M.; Doré, O.; Douspis, M.; Ducout, A.; Dupac, X.; Dusini, S.; Efstathiou, G.; Elsner, F.; Enßlin, T. A.; Eriksen, H. K.; Fantaye, Y.; Farhang, M.; Fergusson, J.; Fernandez-Cobos, R.; Finelli, F.; Forastieri, F.; Frailis, M.; Fraisse, A. A.; Franceschi, E.; Frolov, A.; Galeotta, S.; Galli, S.; Ganga, K.; Génova-Santos, R. T.; Gerbino, M.; Ghosh, T.; González-Nuevo, J.; Górski, K. M.; Gratton, S.; Gruppuso, A.; Gudmundsson, J. E.; Hamann, J.; Handley, W.; Hansen, F. K.; Herranz, D.; Hildebrandt, S. R.; Hivon, E.; Huang, Z.; Jaffe, A. H.; Jones, W. C.; Karakci, A.; Keihänen, E.; Keskitalo, R.; Kiiveri, K.; Kim, J.; Kisner, T. S.; Knox, L.; Krachmalnicoff, N.; Kunz, M.; Kurki-Suonio, H.; Lagache, G.; Lamarre, J. M.; Lasenby, A.; Lattanzi, M.; Lawrence, C. R.; Le Jeune, M.; Lemos, P.; Lesgourgues, J.; Levrier, F.; Lewis, A.; Liguori, M.; Lilje, P. B.; Lilley, M.; Lindholm, V.; López-Caniego, M.; Lubin, P. M.; Ma, Y. Z.; Macías-Pérez, J. F.; Maggio, G.; Maino, D.; Mandolesi, N.; Mangilli, A.; Marcos-Caballero, A.; Maris, M.; Martin, P. G.; Martinelli, M.; Martínez-González, E.; Matarrese, S.; Mauri, N.; McEwen, J. D.; Meinhold, P. R.; Melchiorri, A.; Mennella, A.; Migliaccio, M.; Millea, M.; Mitra, S.; Miville-Deschênes, M. A.; Molinari, D.; Montier, L.; Morgante, G.; Moss, A.; Natoli, P.; Nørgaard-Nielsen, H. U.; Pagano, L.; Paoletti, D.; Partridge, B.; Patanchon, G.; Peiris, H. V.; Perrotta, F.; Pettorino, V.; Piacentini, F.; Polastri, L.; Polenta, G.; Puget, J. L.; Rachen, J. P.; Reinecke, M.; Remazeilles, M.; Renzi, A.; Rocha, G.; Rosset, C.; Roudier, G.; Rubiño-Martín, J. A.; Ruiz-Granados, B.; Salvati, L.; Sandri, M.; Savelainen, M.; Scott, D.; Shellard, E. P. S.; Sirignano, C.; Sirri, G.; Spencer, L. D.; Sunyaev, R.; Suur-Uski, A. S.; Tauber, J. A.; Tavagnacco, D.; Tenti, M.; Toffolatti, L.; Tomasi, M.; Trombetti, T.; Valenziano, L.; Valiviita, J.; Van Tent, B.; Vibert, L.; Vielva, P.; Villa, F.; Vittorio, N.; Wand elt, B. D.; Wehus, I. K.; White, M.; White, S. D. M.; Zacchei, A., and Zonca, A. Planck 2018 results. VI. Cosmological parameters. *arXiv e-prints*, art. arXiv:1807.06209, 2018.

Scannapieco, C.; Wadepuhl, M.; Parry, O. H.; Navarro, J. F.; Jenkins, A.; Springel, V.; Teyssier, R.; Carlson, E.; Couchman, H. M. P.; Crain, R. A.; Dalla Vecchia, C.; Frenk, C. S.; Kobayashi, C.; Monaco, P.; Murante, G.; Okamoto, T.; Quinn, T.; Schaye, J.; Stinson, G. S.; Theuns, T.; Wadsley, J.; White, S. D. M., and Woods, R. The Aquila comparison project: the effects of feedback and numerical methods on simulations of galaxy formation. *Monthly Notices of the RAS*, 423(2):1726–1749, 2012. doi:10.1111/j.1365-2966.2012.20993.x.

Schaye, Joop. Model-independent Insights into the Nature of the Lyα Forest and the Distribution of Matter in the Universe. *Astrophysical Journal*, 559(2):507–515, 2001. doi:10.1086/322421.

Schaye, Joop. Star Formation Thresholds and Galaxy Edges: Why and Where. *Astrophysical Journal*, 609(2):667–682, 2004. doi:10.1086/421232.

Schaye, Joop and Dalla Vecchia, Claudio. On the relation between the Schmidt and Kennicutt-Schmidt star formation laws and its implications for numerical simulations. *Monthly Notices of the RAS*, 383(3):1210–1222, 2008. doi:10.1111/j.1365-2966.2007.12639.x.

Schaye, Joop; Crain, Robert A.; Bower, Richard G.; Furlong, Michelle; Schaller, Matthieu; Theuns, Tom; Dalla Vecchia, Claudio; Frenk, Carlos S.; McCarthy, I. G.; Helly, John C.;

Jenkins, Adrian; Rosas-Guevara, Y. M.; White, Simon D. M.; Baes, Maarten; Booth, C. M.; Camps, Peter; Navarro, Julio F.; Qu, Yan; Rahmati, Alireza; Sawala, Till; Thomas, Peter A., and Trayford, James. The EAGLE project: simulating the evolution and assembly of galaxies and their environments. *Monthly Notices of the RAS*, 446(1): 521–554, 2015. doi:10.1093/mnras/stu2058.

Schmidt, Maarten. The Rate of Star Formation. *Astrophysical Journal*, 129:243, 1959. doi:10.1086/146614.

Somerville, Rachel S. and Davé, Romeel. Physical Models of Galaxy Formation in a Cosmological Framework. *Annual Review of Astron and Astrophys*, 53:51–113, 2015. doi:10.1146/annurev-astro-082812-140951.

Springel, Volker. E pur si muove: Galilean-invariant cosmological hydrodynamical simulations on a moving mesh. *Monthly Notices of the RAS*, 401(2):791–851, 2010. doi:10.1111/j.1365-2966.2009.15715.x.

Springel, Volker and Hernquist, Lars. Cosmological smoothed particle hydrodynamics simulations: a hybrid multiphase model for star formation. *Monthly Notices of the RAS*, 339(2):289–311, 2003. doi:10.1046/j.1365-8711.2003.06206.x.

Vogelsberger, Mark; Genel, Shy; Sijacki, Debora; Torrey, Paul; Springel, Volker, and Hernquist, Lars. A model for cosmological simulations of galaxy formation physics. *Monthly Notices of the RAS*, 436(4):3031–3067, 2013. doi:10.1093/mnras/stt1789.

Vogelsberger, Mark; Genel, Shy; Springel, Volker; Torrey, Paul; Sijacki, Debora; Xu, Dandan; Snyder, Greg; Nelson, Dylan, and Hernquist, Lars. Introducing the Illustris Project: simulating the coevolution of dark and visible matter in the Universe. *Monthly Notices of the RAS*, 444(2):1518–1547, 2014. doi:10.1093/mnras/stu1536.

Vogelsberger, Mark; Marinacci, Federico; Torrey, Paul, and Puchwein, Ewald. Cosmological simulations of galaxy formation. *Nature Reviews Physics*, 2(1):42–66, 2020. doi:10.1038/s42254-019-0127-2.

Weinberger, Rainer; Springel, Volker, and Pakmor, Rüdiger. The Arepo public code release. *arXiv e-prints*, art. arXiv:1909.04667, 2019.

Williams, Thomas G.; Gear, Walter K., and Smith, Matthew W. L. The star formation law at GMC scales in M33, the Triangulum galaxy. *Monthly Notices of the RAS*, 479 (1):297–314, 2018. doi:10.1093/mnras/sty1476.